

First-Principles Study of Pyroxene Structure LiVO_3

Mohamed Khedidji*

Department of Chemistry, Theoretical Chemistry and Computational Photonics Laboratory, University of Science and Technology, Houari Boumediene, BP 32 El-Alia, Algiers, 16111, Algeria

ABSTRACT

In order to study the possible occurrence of the ferroelectric-paraelectric phase transition in the monoclinic LiVO_3 , which remains experimentally ambiguous, we performed first-principles computations of the structural, dielectric and dynamical properties of LiVO_3 in its high-temperature paraelectric structure of $C2/c$ symmetry. The results show that LiVO_3 exhibits three unstable phonon modes, which, after their condensation, lead to more stable phases of low symmetry. The obtained ground state phase is not ferroelectric, it is a non-polar phase of $P2_{1/c}$ symmetry. However, the condensation of a low frequency mode obtained at 14 cm^{-1} leads to the ferroelectric phase of Cc symmetry, which confirms that the ferroelectric-paraelectric phase transition is possible for monoclinic LiVO_3 , which can then be controlled by applying an external parameter.

Keywords: Pyroxene; DFT; Phonons; Phase transition; Oxide

Abbreviations: LIBs: Lithium-Ion Batteries; EV: Electric Vehicles; HEV: Hybrid Electric Vehicles; DFT: Density Functional Theory; GGA: Generalized Gradient Approximation; ONCV: Optimized Norm-Conserving Vanderbilt pseudopotentials; DFPT: Density-Functional Perturbation Theory

INTRODUCTION

The switchable macroscopic polarization characteristic of ABO_3 -type ferroelectric materials makes them good candidates for modern devices such as pyroelectric detectors, binary memories and electro-optic modulators for communication systems [1-4]. The Lithium Vanadium (LiVO_3) is one of these materials, widely used in the manufacturing of modern devices. It has been qualified to be used as solid electrolyte material as well as composite cathode for rechargeable Lithium-Ion Batteries (LIBs) used for Electric Vehicles (EV) and Hybrid Electric Vehicles (HEV) [5,6].

Due to the high mobility of Li^+ cation, the unidimensional character of its structure and its electrochemical characteristics, LiVO_3 appears as an important ferroelectric material which has been studied intensively in the past years [7-11]. LiVO_3 belongs to the class of metavanadate pyroxenes family of the type MVO_3 ($\text{M}=\text{Li}, \text{Na}, \text{K}, \text{Rb}$ and Cs), in which infinite chains of corner shared VO_4 tetrahedra, interconnected through MO_6 octahedra. The experimental studies showed that LiVO_3 must undergoes a ferroelectric-paraelectric phase transition at about 410°C from the Cc polar phase to the $C2/c$ centrosymmetric phase [12,13].

By mean of high-resolution Neutron Powder Diffraction method, Muller, et al. [13], have associated this kind of phase transition to the reorientation of the anisotropic displacement ellipsoids of the lithium atoms around their average sites. This slight modification in structure introduced a symmetry problem in several experimental studies. Therefore, a detailed knowledge of ferroelectricity and phase transition mechanisms in LiVO_3 is still remains obscure.

In the present work, we investigate the structural, dielectric and dynamical properties of monoclinic LiVO_3 , using first-principles methods. We study and discuss the possible occurrence of the $C2/c$ - Cc ferroelectric phase transition. The condensation of the obtained phonon instabilities reveal that the $P2_{1/c}$ phase, obtained from the condensation of the unstable γ_2^+ mode into the paraelectric $C2/c$ phase, is the ground state phase. In addition, the condensation of the stable polar mode Γ_2^- into the paraelectric $C2/c$ phase leads to the ferroelectric phase of Cc symmetry. This means that the ferroelectric phase transition remains possible for monoclinic LiVO_3 . Finally, the spontaneous polarization of such a ferroelectric phase is then calculated using two methods: The Berry phase formalism and from the knowledge of the born effective charge and the dielectric tensor.

Correspondence to: Mohamed Khedidji, Department of Chemistry, Theoretical Chemistry and Computational Photonics Laboratory, University of Science and Technology, Houari Boumediene, BP 32 El-Alia, Algiers, 16111, Algeria, E-mail: khedidjimohammed29@gmail.com

Received: 11-Feb-2022, Manuscript No. JPCB-22-15748; **Editor assigned:** 14-Feb-2022, PreQC No. JPCB-22-15748 (PQ); **Reviewed:** 28-Feb-2022, QC No. JPCB-22-15748; **Revised:** 07-Mar-2022, Manuscript No. JPCB-22-15748 (R); **Published:** 14-Mar-2022, DOI: 10.35248/2161-0398.22.S1.003.

Citation: Khedidji M (2022) First-Principles Study of Pyroxene Structure LiVO_3 . J Phys Chem Biophys. S1:003.

Copyright: © 2022 Khedidji M. This is an open-access article distributed under the terms of the Creative Commons Attribution License, which permits unrestricted use, distribution, and reproduction in any medium, provided the original author and source are credited.

MATERIALS AND METHODS

Computational details

Our calculations were performed in the general framework of the Density Functional Theory (DFT) [14,15]. Using plane-wave pseudopotentials method as implemented in the ABINIT software package [16,17]. We chose the Generalized Gradient Approximation (GGA) [18], as exchange-correlation functional. Optimized Norm-Conserving Vanderbilt pseudopotentials (ONCV) were used to represent the core region of lithium, vanadium and oxygen atoms [19]. The V (3s 3p 3d), Li (2s) and O (2s 2p) levels, were considered as valence states in the generation of the pseudopotentials. Wave functions were extended in plane waves up to a kinetic energy cutoff of 45 Ha. The Brillouin zone was sampled with a $4 \times 5 \times 6$ Monkhorst-Pack k-point grid converges the results very well [20]. We relaxed the structure until the remaining forces on the atoms are less than 10^{-5} Hartree/Bohr and the stresses on the unit cell are smaller than 10^{-7} . Phonons frequencies, Born effective charges and dielectric tensors were computed using Density-Functional Perturbation Theory (DFPT) [21,22].

RESULTS AND DISCUSSION

Structure

We first determined the structural parameters of the experimentally observed High-temperature paraelectric C2/c phase of LiVO_3 by relaxing simultaneously the unit cell shape and the atomic positions. The C2/c structure has 40 atoms per conventional unit cell or 20 atoms in the primitive unit cell. The crystal structure, as shown on Figure 1, exhibits the altering chains of VO_4 tetrahedra (gray) and distorted LiO_6 octahedra (blue). This structure consists of bands of V-O corner-shared tetrahedra run parallel to c-axis and is interconnected through edge-shared LiO_6 octahedra which also run parallel to this axis. Our results after full structural optimization are listed on Table 1. Except of the typical error of the GGA method that is known to overestimate the lattice parameters, the results are in good agreement with the experiment.

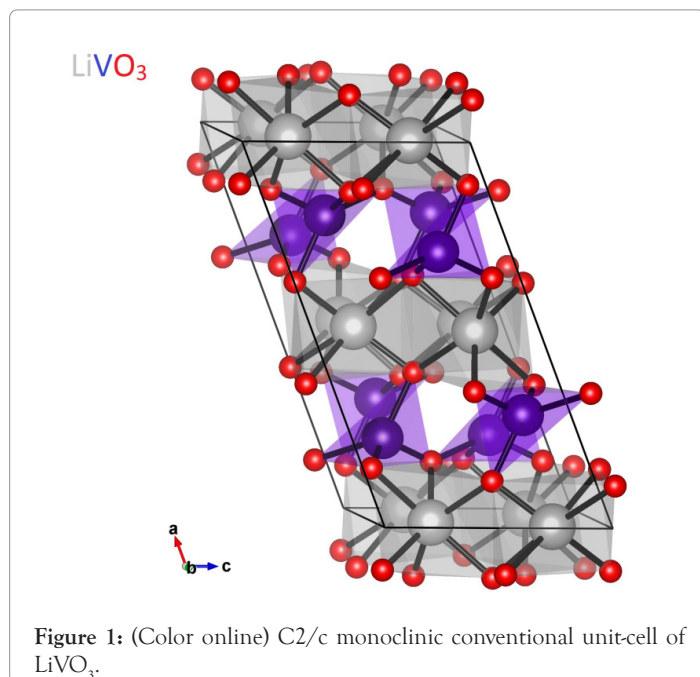


Table 1: Calculated lattice parameters and atomic positions of LiVO_3 in the C2/c monoclinic phase. In parentheses are the experimental values reported here from [13].

Atom	Wyckoff	x	y	z
Li_1	4e	0	0.9148	0.25
		0	0.9267	0.25
Li_2	4e	0	0.2673	0.25
		0	0.2831	0.25
V	8f	0.2887	0.0933	0.2739
		0.287	0.084	0.265
O_1	8f	0.1159	0.1084	0.1689
		0.1141	0.1112	0.166
O_2	8f	0.352	0.2346	0.2894
		0.3563	0.2723	0.2819
O_3	8f	0.3582	-0.0291	0.0857
		0.3548	-0.0276	0.0762
$a = 10.3348 \text{ \AA}$ (10.1616)	$b = 8.6362 \text{ \AA}$ (8.4281)	$c = 5.8897 \text{ \AA}$ (5.8863)	$\beta = 111.1900$ (110.4660)	

Dielectric properties

The born effective charge (Z^*) and the optical dielectric tensor (ϵ_∞) are important and central for the parameterization of the LO-TO splitting that is considered as the contribution of the long range coulomb interactions to the lattice dynamics. These two quantities have been computed using linear-response techniques [22]. The elements of the calculated ϵ_∞ tensor are reported in Cartesian coordinates with the x and y axes aligned along the a and b directions of C2/c structure, respectively, and the z axis makes an angle of $(\beta-\pi/2)$ with the c direction. Within this choice of Cartesian axes, the ϵ_∞ tensor is blocking diagonal in y and xz subspaces;

$$\begin{pmatrix} 3.47 & 0 & -0.29 \\ 0 & 3.57 & 0 \\ -0.29 & 0 & 4.11 \end{pmatrix}$$

Neither experimental nor theoretical values to compare our results. It is well known that, for the dielectric tensor, the calculated values always overestimate the experimental one.

Table 2 shows the calculated Z^* tensors for non-equivalents atoms. The Z^* tensors are reported in Cartesian coordinates using the same set of axes as used for the dielectric tensor. The C2/c symmetry of LiVO_3 requires that the Z^* tensor should be anisotropic on each atom, so that the charge transfer takes place in different directions. Moreover, all the calculated Z^* values are close to their corresponding nominal charges, which, contrast with what is observed for the class of ferroelectric perovskites that exhibit anomalous Z^* [23].

Dynamical properties

To study the structural instabilities in the monoclinic C2/c configuration of LiVO_3 , we performed zone-center phonon calculations in the conventional cell of 40 atoms (Figure 1). In this configuration the Brillouin zone is folding, and so gives access to phonons at Γ (0, 0, 0) and $Y=(0, 1, 0)$ points. We obtained three unstable modes. The strongest unstable mode is at $61i \text{ cm}^{-1}$ and corresponding to the irreducible representation Γ_2^- . The two remaining unstable modes are at $57i \text{ cm}^{-1}$ and $24i \text{ cm}^{-1}$ and corresponding to the irreducible representation Y_2^- and Y_2^- , respectively (Table 3).

Table 2: Born effective charges calculated for monoclinic LiVO_3 . The nominal charges of Li, V and O are +1, +5 and -2, respectively.

Atom	Z_{xx}^*	Z_{xy}^*	Z_{xz}^*	Z_{yx}^*	Z_{yy}^*	Z_{yz}^*	Z_{zx}^*	Z_{zy}^*	Z_{zz}^*
Li ₁	1.64	0	0.15	0	1.41	0	0.22	0	1.17
Li ₂	1.5	0	0.26	0	1.17	0	0.22	0	1.06
V	3.14	0.2	-0.72	-0.09	3.4	-0.64	-0.76	0.26	4.71
O ₁	-1.23	0.59	1.09	0.77	-1.5	-1.68	1.03	-1.23	-3.82
O ₂	-2.4	0.32	-0.53	0.14	-0.94	-0.02	-0.48	0.24	-1.08
O ₃	-1.08	0.73	-0.03	0.83	-2.23	0.21	0	0.03	-0.93

Note: * Born effective charge.

Table 3: Calculated eigendisplacements (in a.u.) of unstable TO modes. Atomic displacements corresponding to polar mode Γ_2^- are also reported. The values in brackets present the frequencies of different modes in cm^{-1} .

Atom	Γ_2^+ (61i)			Y_2^+ (57i)		
	x	y	z	X	y	z
Li ₁	0.0043	0	0.0367	0.0052	0	-0.0263
Li ₂	-0.0314	0	-0.1173	0.0043	0	0.1031
V	-0.0058	-0.0185	0.0003	0.0096	0.0206	0.0017
O ₁	-0.0072	0.0151	-0.0015	0	0.0313	-0.0041
O ₂	-0.0118	-0.0122	0.0133	0.0124	-0.0074	0.0021
O ₃	-0.0247	-0.0267	-0.0326	0.0275	0.027	0.0315

Atom	Y_2^+ (24i)			Γ_2^- (14i)		
	x	y	z	x	y	z
Li ¹	0.0179	0	0.0254	0.0027	0	0.088
Li ₂	0.0087	0	0.0871	0.0396	0	0.1359
V	-0.0056	-0.0106	-0.0096	0.0096	-0.0011	-0.0042
O ₁	0.0051	-0.0364	0.0247	0.0061	-0.0048	-0.0016
O ₂	-0.0019	0.0313	-0.0058	0.0057	0.006	-0.006
O ₃	0.0031	0.0074	0.0483	-0.002	-0.0053	-0.0352

In order to study the symmetry-breaking behavior of $C2/c$ monoclinic LiVO_3 , we first individually condensed the three unstable modes into the $C2/c$ parent phase and then we fully optimized the aroused distorted phases. We ported on Table 4 the low-symmetry phases with their corresponding cell parameters obtained after full relaxation and their energy differences (ΔE_m) calculated with respect to the $C2/c$ parent structure. The condensation of mode Γ_2^+ leads to a triclinic structure of space group $P\bar{1}$. While, the condensation of the nonpolar modes Y_2^+ and Y_2^- lead to a monoclinic structure

of space group $P2_{1/c}$. Also, the calculated ΔE_m show that the $P2_{1/c}$ phase arising from the condensation of Y_2^+ mode is the most stable phase because it exhibits the lowest ΔE_m , with an important energy gain of about 150 meV/f.u. Significantly, as shown on Table 4, the condensation of the stable polar mode Γ_2^- into the $C2/c$ paraelectric phase leads to a ferroelectric phase of Cc symmetry. Despite numerous experimental efforts, this phase transition is still ambiguously stated. This is probably due to the very small structural changes between Cc and $C2/c$ phases [13].

Table 4: Cell parameters (lengths in Å and angles in $^\circ$), energy differences ΔE_m (in meV/f.u) and space groups of different phases obtained after condensation of unstable modes.

Mode	Symmetry	Cell parameters	ΔE_m
Γ_2^+	$P\bar{1}$	a=10.72, b=9.12, c=5.80 $\alpha=94, \beta=144, \gamma=81$	-57.43
Y_2^+	$P2_{1/c}$	a=10.34, b=8.83, c=5.83 $\alpha=\gamma=90, \beta=114$	-20.65
Y_2^-	$P2_{1/c}$	a=11.12, b=11.76, c=5.64 $\alpha=\gamma=90, \beta=120$	-20.65
Γ_2^-	Cc	a=10.33, b=8.76, c=5.89 $\alpha=\gamma=90, \beta=110$	-0.5

Spontaneous polarization

According to the modern theory of polarization [24], the spontaneous polarization of bulk LiVO_3 is well attributed to a formal transformation from a paraelectric $C2/c$ structure to a polar Cc structure. The Cc symmetry of LiVO_3 allows a development of a spontaneous polarization along the x and z axes. To calculate this fundamental quantity we used both the Berry Phase approach (BP) [24], and from the knowledge of the born effective charges and atomic displacements as;

$$P_{s,\alpha} = \frac{e}{\Omega} \sum_{k,\beta} Z_{k,\alpha\beta}^* \delta\tau_{k,\beta}$$

where $Z_{k,\alpha\beta}^*$ is the born effective charge tensor of atom k and $\delta\tau_{k,\beta}$ presents the displacement of such atom along the direction β during the phase transition from the paraelectric $C2/c$ phase to the ferroelectric Cc phase. This estimation gives $3.19 \mu\text{C}/\text{cm}^2$ along the x direction and $7.28 \mu\text{C}/\text{cm}^2$ along the z direction. From BF formalism, the computed spontaneous polarization is of $5.80 \mu\text{C}/\text{cm}^2$ and $7.56 \mu\text{C}/\text{cm}^2$ along the x and z directions, respectively. Finally, we observe that the $P_s(Z^*)$ underestimates $P_s(\text{BP})$ along the a direction, while along the c direction $P_s(Z^*)$ is in closer agreement with $P_s(\text{BF})$.

CONCLUSION

We have performed a systematical study of structural, dielectric and dynamical properties of LiVO_3 in its high-temperature paraelectric structure of $C2/c$ symmetry using density functional theory and density functional perturbation theory. We characterized the $C2/c$ high-temperature structure. Dielectric properties and phonon frequencies were calculated. Unlike typical perovskites, the computed Z^* are not anomalous and are close to their nominal values. A phonons calculation reveals three structural instabilities that lead after their condensation to more stable phases of monoclinic and triclinic symmetries. The ground state phase is monoclinic of $P2_1/c$ symmetry. Finally, the condensation of the polar mode at 14 cm^{-1} leads to the polar phase of Cc symmetry, which confirms the possible occurrence of the ferroelectric-paraelectric phase transition.

REFERENCES

1. Lines ME, Glass AM. Principles and applications of ferroelectrics and related materials. Oxford Classic Texts in the Physical Sciences, Clarendon Press, Oxford. 1977.
2. Nishihara, Haruna M, Suhara T. Optical integrated circuits, edited by RE Fischer and WJ Smith, optical and electro-optical engineering series. Mcgraw-Hill, New York. 1985.
3. Wooten EL, Kissa KM, Yi-Yan A, Murphy EJ, Lafaw DA, Hallemeier PF, et al. A review of lithium niobate modulators for fiber-optic communications systems. IEEE J Sel Top Quantum Electron. 2000;6(1):69-82.
4. Buse K, Adibi A, Psalti D. Non-volatile holographic storage in doubly doped lithium niobate crystals. Nature. 1998;393(6686):665-668.
5. Huang Z, Cao L, Kuang Y, Zhou H, Fu C, Chen Z. Preparation, characterization, and lithium intercalation behavior of LiVO_3 cathode material for lithium-ion batteries. J Phys Chem C. 2016;120(6):3242-3429.
6. Lee JB, Moon J, Chae OB, Lee JG, Ryu JH, Cho M, et al. Unusual conversion-type lithium in LiVO_3 electrode for lithium-ion batteries. Chem Mater. 2016;28(15):5314-5320.
7. Jian XM, Tu JP, Qiao YQ, Lu Y, Wang XL, Gu CD. Synthesis and electrochemical performance of LiVO_3 cathode materials for lithium ion batteries. J Power Sources. 2013;236:33-38.
8. Jian JB, Wenren HQ, Huang S, Shi SJ, Wang XL, Gu CD, et al. Oxalic acid-assisted combustion synthesized LiVO_3 cathode material for lithium ion batteries. J Power Sources. 2014;246:417-422.
9. Li P, Ren X, Guo GC, He L. The origin of hyperferroelectricity in LiBO_3 ($B = V, Nb, Ta, Os$). Sci Rep. 2016;6:34085.
10. Li S, Zhang Y, Tang Y, Tan X, Liang S, Zhou J. Facile synthesis of LiVO_3 and its electrochemical behavior in rechargeable lithium batteries. J Electroanal Chem. 2019;853:113505.
11. Khedidji M, Amoroso D, Djani H. Microscopic mechanisms behind hyperferroelectricity. Phys Rev B. 2021;103(1):014116.
12. Kashid AP, Patil VV, Chavan SH. Pyroelectric properties of Gd-doped KVO_3 and LiVO_3 . Bull Mater Sci. 1989;12(1):57-62.
13. Muller C, Valmalette JC, Soubeyrou JL, Bouree F, Gavarrri JR. Structural disorder and ionic conductivity in LiVO_3 : A neutron powder diffraction study from 340 to 890 K. J Solid State Chem. 2001;156(2):379-389.
14. Hohenberg P, Kohn W. Inhomogeneous electric gas. Phys Rev B. 1964;136(3B):B864.
15. Kohn W, Sham LJ. Self-consistent equations including exchange and correlation effects. Phys Rev B. 1965;140(4A):A1133.
16. Gonze X, Amadon B, Anglade PM, Beuken JM, Bottin F, Boulanger P, et al. ABINIT: First-principles approach to material and nanosystem properties. Comput Phys Commun. 2009;180(12):2582-2615.
17. Gonze X, Beuken JM, Caracas R, Detraux F, Fuchs M, Rignanese GM, et al. First-principles computation of material properties: The ABINIT software project. Comput Mater Sci. 2002;25(3):478-492.
18. Perdew JP, Burke K, Ernzerhof M. Generalized gradient approximation made simple. Phys Rev Lett. 1996;77:3865-3868.
19. Hamann DR. Optimized norm-conserving vanderbilt pseudopotentials. Phys Rev B. 2013;88(8):085117.
20. Monkhorst HJ, Pack JD. Special points for brillouin-zone integrations. Phys Rev B. 1976;13(12):5188.
21. Baroni S, De Gironcoli S, Dal Corso A, Giannozzi P. Phonons and related crystal properties from density-functional perturbation theory. Rev Mod Phys. 2001;73:515.
22. Gonze X, Lee C. Dynamical matrices, born effective charges, dielectric permittivity tensor, and interatomic force constants from density-functional perturbation theory. Phys Rev B. 1997;55(16):10355.
23. Ghosez P, Michenaud JP, Gonze X. Dynamical atomic charges: The case of ABO_3 compounds. Phys Rev B. 1998;58(10):6224.
24. Resta R. Macroscopic polarization in crystalline dielectrics: The geometric phase approach. Rev Mod Phys. 1994;66(3):899.